European Journal of Nuclear Medicine and Molecular Imaging (2019) 46:2051–2064
https://doi.org/10.1007/s00259-019-04369-6

ORIGINAL ARTICLE

[^{11}C]JNJ54173717, a novel P2X7 receptor radioligand as marker for neuroinflammation: human biodistribution, dosimetry, brain kinetic modelling and quantification of brain P2X7 receptors in patients with Parkinson's disease and healthy volunteers

Donatienne Van Weehaeghe[1] · Michel Koole[1] · Mark E. Schmidt[2] · Stephanie Deman[3,4] · Andreas H. Jacobs[5,6] · Erika Souche[3,4] · Kim Serdons[1] · Stefan Sunaert[7] · Guy Bormans[8] · Wim Vandenberghe[9,10] · Koen Van Laere[1]

Received: 24 January 2019 / Accepted: 23 May 2019 / Published online: 26 June 2019

Abstract

Purpose The P2X7 receptor (P2X7R) is an ATP-gated ion channel predominantly expressed on activated microglia and is important in neurodegenerative diseases including Parkinson's disease (PD). In this first-in-human study, we investigated [^{11}C]JNJ54173717 ([^{11}C]JNJ717), a selective P2X7R tracer, in healthy volunteers (HV) and PD patients. Biodistribution, dosimetry, kinetic modelling and short-term test–retest variation (TRV), as well as possible genotype effects, were investigated.

Methods Biodistribution and radiation dosimetry studies were performed in three HV (mean age 30 ± 2 years, two women) using whole-body PET/CT. The most appropriate kinetic model was determined in 11 HV (mean age 62 ± 10 years, six women) and 10 PD patients (mean age 64 ± 8 years, three women; mean UPDRS motor score 21 ± 8) using 90-min dynamic simultaneous PET/MR scans. The total volume of distribution (V_T) was calculated using a one-tissue and a two-tissue compartment model (1TCM, 2TCM) and Logan graphical analysis, and its time stability was assessed. Seven subjects underwent retest scans (mean age 60 ± 13 years, four HV, one woman). A group analysis was performed to compare PD patients and HV. Finally, 13 exons of P2X7R were genotyped in all subjects included in the second part of the study.

Results The mean effective dose was 4.47 ± 0.32 μSv/MBq, with the highest absorbed doses to the gallbladder, liver and small intestine. A reversible 2TCM was the most appropriate kinetic model with relatively homogeneous V_T values in the grey and white matter. Average V_T values were 3.4 ± 0.8 in HV and 3.3 ± 0.7 in PD patients, with no significant difference between the groups, but a possible genotype effect (rs3751143) was identified which can affect V_T. Average TRV was 10–15%. The stability of V_T over time allowed a reduction in scan time to 70 min.

Conclusion [^{11}C]JNJ717 is safe and suitable for quantifying P2X7R expression in human brain. In this pilot study, no significant differences in P2X7R binding were found between HV and PD patients. The results also suggest that genotype effects need to be incorporated in future P2X7R PET analyses.

This article is part of the Topical Collection on Neurology

Electronic supplementary material The online version of this article (https://doi.org/10.1007/s00259-019-04369-6) contains supplementary material, which is available to authorized users.

✉ Donatienne Van Weehaeghe
donatienne.vanweehaeghe@uzleuven.be

[1] Division of Nuclear Medicine and Molecular Imaging, University Hospitals of Leuven and KU Leuven, Leuven, Belgium

[2] Janssen Research and Development: Beerse, Beerse, Belgium

[3] Genomics Core, UZ Leuven, Leuven, Belgium

[4] Department of Human Genetics, KU Leuven, Leuven, Belgium

[5] European Institute for Molecular Imaging (EIMI), Westfalian Wilhelms University (WWU) Münster, Münster, Germany

[6] Department of Geriatrics and Neurology, Johanniter Hospital Bonn, Bonn, Germany

[7] Department of Radiology, University Hospitals Leuven, Gasthuisberg, UZ, Leuven, Belgium

[8] Laboratory for Radiopharmaceutical Research, KU Leuven, Leuven, Belgium

[9] Department of Neurosciences, KU Leuven, Leuven, Belgium

[10] Department of Neurology, University Hospitals Leuven, Leuven, Belgium

Keywords P2X7 receptor · Neuroinflammation PET · Parkinson · Dosimetry · Genotyping · [^{11}C]JNJ54173717

Introduction

Activated microglia are a hallmark of neuroinflammation and are thought to play a central role in the pathogenesis and progression of neurodegenerative diseases such as Parkinson's disease (PD), Alzheimer's disease and amyotrophic lateral sclerosis (ALS) [1]. The purinergic P2X7 receptor (P2X7R), an adenosine triphosphate (ATP)-gated ion channel, is expressed mainly on activated microglia throughout the brain and spinal cord [2, 3]. However, low P2X7R expression is also present on neurons, astrocytes and oligodendrocytes as 17% of the P2X7R mRNA signal remained in hippocampal slice cultures depleted of microglia [4]. Stimulation of P2X7R initiates the release of proinflammatory cytokines such as IL-1β and IL-18 by promoting the NLPR3 inflammasome assembly [5]. Furthermore, preclinical data from a mouse model of Alzheimer's disease showed that P2X7R antagonism reduces the formation of hippocampal amyloid plaques, resulting in reduced cognitive impairment and improved dendritic spine development [6, 7]. In a rat model of PD, P2X7R antagonism increased tyrosine hydroxylase immunoreactivity and decreased loss of nigral dopaminergic neurons such that hemiparkinsonism was partially reversed [8, 9]. In a mouse model of ALS, motor coordination was improved by P2X7R antagonism while weight loss was delayed and survival increased [10]. On the other hand, in P2X7R knockout mice with toxin-induced parkinsonism, no neuroprotective effect was observed [11]. Moreover, exacerbation of pathology was found in mouse models of ALS [12]. Also in a post-mortem study, the importance of P2X7R was shown as an increase (about twofold) in P2X7R immunoreactivity in the spinal cord of patients with ALS and multiple sclerosis compared to controls, although the cause of death was not taken into account in that study as a potential confounder [13].

Accordingly, in vivo visualization and quantification of P2X7R in the brain is of great importance in the study of the pathogenesis of human neurodegenerative disorders and to allow therapeutic drug monitoring. Recently, a ^{18}F-labelled P2X7R compound ([^{18}F]JNJ64413739) with acceptable (±10%) test–retest variation (TRV) for a 90-min acquisition protocol was developed. However, ^{11}C compounds could be beneficial as they would facilitate 1-day scan protocols such as dose occupancy studies. In collaboration with Janssen Pharmaceuticals, a promising ^{11}C-P2X7R radiotracer [^{11}C]JNJ54173717 ([^{11}C]JNJ717) was developed that shows a nanomolar affinity for human P2X7R (K_D = 1.6 nM). The selectivity and kinetics of [^{11}C]JNJ717 were investigated in a rat model with local brain lentiviral overexpression of human P2X7R and in monkeys, and negligible nonspecific binding and good blood–brain barrier permeability were shown [14].

In this first-in-human study, we investigated the biodistribution, dosimetry, kinetic modelling and short-term TRV of [^{11}C]JNJ717 in a set of healthy volunteers (HV) and PD patients. Secondly, we investigated differences between 10 PD patients and 11 age-matched HV with regard to P2X7R distribution and structural changes. We also examined a possible genotype effect on binding affinity and expression level as the human P2X7R is highly polymorphic [15].

Materials and methods

Study design and objectives

HV were recruited in response to advertisements on the internet and departmental websites. The main exclusion criteria included: abnormal physical or neurological examination or paraclinical investigations, history of significant medical illnesses including major internal pathology or neurological and neuropsychiatric disorders, history of clinically relevant drug or food allergies, and chronic or acute use (if shortly before a scan) of antiinflammatory medication such as nonsteroidal antiphlogistics and systemic corticosteroids. Inclusion criteria for PD patients included: older than 45 years and diagnosis of PD according to UK Brain Bank criteria with at least two main symptoms (resting tremor, bradykinesia or rigidity). In total 14 HV and 10 PD patients were included in the two parts of the study. In the first part dosimetry was performed, and in the second part kinetic modelling was performed, TRV was determined and the groups were compared. Demographic data and tracer information for each part of the study are summarized in Table 1. Short-term test–retest scans were performed in four HV and three PD patients. PD patients were clinically characterized using the unified Parkinson's disease rating scale (UPDRS) part 3 (motor score) and the Hoehn and Yahr (H&Y) scale on medication. Levodopa-equivalent daily doses were calculated as described previously [16]. The study was approved by the local ethics committee (Ethics Committee UZ/KU Leuven) and was performed in accordance with the principles of the World Medical Association Declaration of Helsinki. Written informed consent was obtained from all subjects prior to the study.

Biodistribution and dosimetry studies

The biodistribution and dosimetry study was performed in three young HV (mean age 30 ± 2 years; two women). Consecutive whole-body (WB) PET/CT scans were obtained

Table 1 Demographics

Subject number	Subject status	Sex	Age (years)	Weight (kg)	PET tracer administered						UPDRS motor score	Hoehn and Yahr stage	Levodopa-equivalent daily dose (mg)
					Dose (MBq)		Mass (μg)		Molar activity (GBq/μmol)				
					Test	Retest	Test	Retest	Test	Retest			
Part 1: Dosimetry													
1	HV	F	27	70	129	–	0.2	–	226	–	–	–	–
2	HV	F	32	63	228	–	2.2	–	45	–	–	–	–
3	HV	M	30	74	210	–	1.6	–	56	–	–	–	–
Part 2: Kinetic modelling, test–retest variation and group comparison													
1	HV	F	55	60	154	–	0.5	–	129	–	–	–	–
2	HV	M	73	70	161	314	2.0	3.1	34	42	–	–	–
3	HV	F	40	68	310	230	3.9	3.1	25	42	–	–	–
4	HV	F	53	78	187	280	0.7	0.7	107	179	–	–	–
5	HV	M	75	70	307	258	4.8	0.9	27	119	–	–	–
6	HV	M	63	114	236	–	0.9	–	115	–	–	–	–
7	HV	M	66	92	325	–	1.0	–	136	–	–	–	–
8	HV	F	53	75	210	–	1.6	–	53	–	–	–	–
9	HV	F	60	66	247	–	0.4	–	233	–	–	–	–
10	HV	F	68	59	302	–	0.9	–	138	–	–	–	–
11	HV	M	69	79	254	–	0.9	–	116	–	–	–	–
12	PD	M	75	83	304	–	0.8	–	165	–	22	1	660
13	PD	M	46	85	134	278	1.3	2.8	44	42	13	1	615
14	PD	M	59	102	216	–	3.5	–	26	–	31	2	605
15	PD	M	62	80	279	222	4.2	2.0	28	46	11	1	505
16	PD	M	69	76	271	211	1.0	0.6	110	211	30	2	250
17	PD	F	60	63	153	–	1.2	–	54	–	13	1	400
18	PD	F	66	50	304	–	0.6	–	231	–	15	1	405
19	PD	F	65	65	228	–	0.4	–	218	–	19	1	205
20	PD	M	73	90	175	–	0.4	–	192	–	34	2	1,840
21	PD	M	58	90	244	–	0.7	–	153	–	25	2	105

HV healthy volunteer, *PD* Parkinson's disease

from the midfemoral position to the head (nine sequential WB scans from tracer injection to 90 min after injection). The mean injected activity was 189 ± 43 MBq with a mean specific (molar) activity of 109 ± 83 GBq/μmol. The WB PET/CT scans were performed on a Hirez Biograph 16 PET/CT system (Siemens, Erlangen, Germany). A vacuum cushion and body strap were used to limit patient movement during scanning. Data were corrected for randoms, scatter and attenuation, and reconstructed using 3D ordered subset expectation maximization (OSEM) iterative reconstruction (five iterations and eight subsets) with correction followed by gaussian postsmoothing with 6-mm full-width at half-maximum (FWHM). A low-dose CT scan was performed prior to the PET scan for attenuation correction.

Normalized cumulated activities (NCA) were calculated by dividing the area under the time–activity curve (TAC) of each source organ by the total injected activity. For the small intestine, and upper and lower large intestine the ICRP 30 gastrointestinal model was used. The fraction entering the small intestine was used as input and set equal to the decay-corrected plateau fraction of injected activity encompassed by the intestinal volume of interest (VOI). Based on the NCAs, absorbed doses were calculated using OLINDA v. 1.1 [17], according to the ICRP 60 [18] definition, and using the Medical Internal Radiation Dose scheme. Effective doses (ED) were calculated from the individual organ doses based on predefined organ weighting factors, as specified by ICRP 60 [18].

Tracer kinetic modelling, test–retest variation and group comparisons

A 90-min dynamic simultaneous PET/MR scan combined with manual arterial blood sampling and tracer radiometabolite analysis was performed in 11 HV (mean age 62 ± 10 years, six women) and 10 PD patients (mean age 64 ± 8 years, three women; UPDRS 33 ± 12; six H&Y stage 1, four H&Y stage 2). All PD patients were on their routine dopaminergic medication in the "ON" state. A retest scan was acquired in 7 of the 21 subjects (mean age 60 ± 13 years, two women, four HV; interscan interval 9 ± 13 days, range 0–28 days). The mean injected activity was 243 ± 54 MBq with a mean specific (molar) activity of 108 ± 69 GBq/μmol.

Data acquisition

PET data were acquired using a General Electric Signa PET/MR system in list mode. Images were reconstructed in 26 frames (4 × 15 s, 4 × 60 s, 2 × 2.5 min, 16 × 5 min) with correction for dead time, randoms, scatter and attenuation. Attenuation correction was performed using a validated zero echo time approach [19]. Reconstructions were performed using 3D OSEM (28 subsets and four iterations), including time of flight information, resolution modelling and in-plane gaussian postsmoothing with 4 mm FWHM. Motion correction was performed using a frame-by-frame approach and rigid coregistration of each frame with the average of the first ten frames (first 10 min of the PET acquisition). To calculate plasma and blood activity curves, 22 arterial blood samples were taken, and six additional arterial blood samples were taken to determine the fraction of parent tracer in arterial plasma and to calculate plasma to whole-blood activity ratios. The activity as determined by gamma counting of high-performance liquid chromatography fractions from the metabolite analysis of plasma samples obtained at 40 and 60 min after injection, showed high standard errors (13.7 ± 5.9% and 48.4 ± 210.3%, respectively). Therefore, all results are given with both individual and average metabolite-corrected input curves. Blood and plasma activity values were fitted to a three-exponential model curve and the plasma metabolite data were fitted to a sigmoid function using PMOD (v. 3.7, PMOD Technologies, Zurich, Switzerland).

At the same time as the PET acquisition, several MR sequences were acquired. A 3D volumetric T1-weighted BRAVO sequence (oblique plane, TE 3.2 ms, TR 8.5 ms, TI 450 ms, flip angle 12°, receiver bandwidth 31.2, number of excitations 1) and a 3D T2-weighted CUBE FLAIR sequence (oblique plane, TE 136 ms, number of echoes 1, echo train length 190, TR 8,500 ms, TI 50 ms, receiver bandwidth 31.25, number of excitations 1) were used.

Data analysis

Composite cortical regions were defined from the N30R83 Hammers atlas in PMOD (v. 3.7) to delineate frontal, temporal, parietal and occipital cortical VOIs (with all cortical regions together constituting a full composite cortical VOI) as well as the cerebellum, striatum, thalamus, hippocampus and corpus callosum [20]. Left and right VOIs were grouped. Subject-specific tissue probability maps for grey and white matter and cerebrospinal fluid were determined using SPM-based multichannel segmentation (SPM12; Wellcome Trust Centre for Neuroimaging, University College, London, UK) using the 3D T1 BRAVO and T2 CUBE FLAIR data. PET/MR data were then spatially normalized to the MNI template using the 3D T1 BRAVO data and three-tissue probability map normalization in PMOD restricted to the subject-specific grey matter part of the whole brain with a fixed threshold of 0.3 (including only voxels with a high probability of belonging to the grey matter). The tissue volumes of distribution (V_T) were calculated using a one-tissue and a two-tissue compartment model (1TCM, 2TCM) and Logan graphical analysis (LGA) (PMOD v. 3.7) with the blood volume fixed to 5% and the equilibration time (t^*) to 36 min. The most appropriate kinetic model was selected using the Akaike information criterion (AIC). This model was then used to evaluate the stability of V_T in relation to the PET acquisition time and the TRV of V_T. TRV was calculated as $2 \times \left(V_{T,i}^{test} - V_{T,i}^{retest}\right) / \left(V_{T,i}^{test} + V_{T,i}^{retest}\right)$ as well as in an absolute way (aTRV) as $2 \times \left|V_{T,i}^{test} - V_{T,i}^{retest}\right| / \left(V_{T,i}^{test} + V_{T,i}^{retest}\right)$, for each brain VOI.

Groups were compared at a cluster level $p_{\mathrm{FWE\text{-}corr}}$ value of <0.05 and peak level p_{height} value of <0.001, and a cluster extent threshold (k_e) of 50 voxels. V_T images were calculated and analysed using both individual and average metabolite-corrected input curves to assess robustness taking the late metabolite sample variation into account. As no significant group atrophy effect was observed between PD patients and HV in a voxel-based morphometry analysis using CAT12 software in SPM (even at a lower threshold: cluster level $p_{\mathrm{uncorr}} < 0.001$, peak level $p_{\mathrm{height}} < 0.005$), PET analyses were performed without partial volume correction.

Genetics

The 13 exons of the P2X7R were all sequenced in venous samples (white blood cells) of the subjects in the second part of the study. Genomic DNA was extracted using a chemagic DNA blood special 4-ml kit (Chemagen-Perkin Elmer, Baesweiler, Germany) on a chemagic

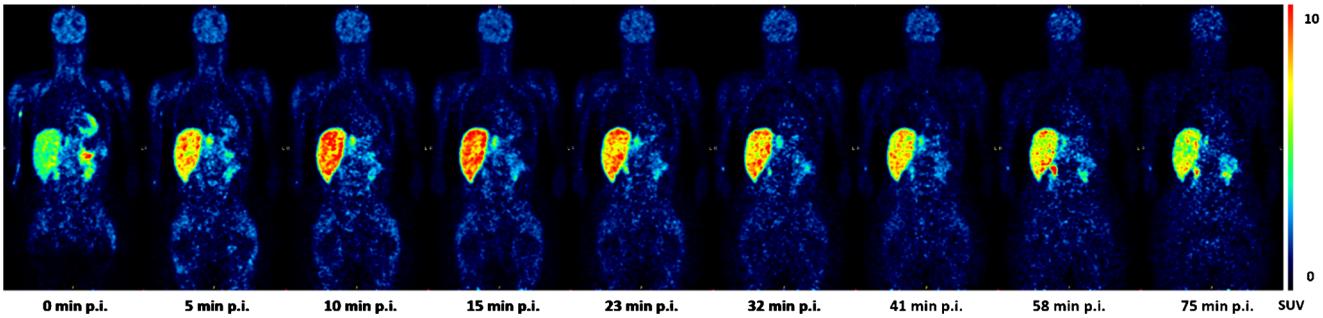

Fig. 1 Representative coronal PET images in subject 1 (Table 1) showing the whole-body time–activity distribution of [^{11}C]JNJ717. The colour intensities are relative to the maximum colour scale indicating SUV shown on the right side to account for physical tracer decay. The start times of the scans (minutes after injection, p.i.) are shown below the images

MSM automate (Chemagen-Perkin Elmer). DNA purity was measured using a DropSense96 (Trinean, Ghent, Belgium) with cDrop software and DNA concentration using the Qubit BR assay. From each sample, 10 µl DNA (10 ng/µl) was used for further analysis.

Molecular inversion probes (MIPs) containing end sequences complementary to the target DNA connected by a 30-base linker sequence were designed, ordered and pooled at 100 µM [21]. After phosphorylation the MIPs were added to the genomic DNA samples to capture the genomic regions of interest. Denaturation of the DNA was followed by hybridization of the probe ends to their complementary target sequence. Complementary bases were incorporated using a DNA polymerase in the gap between the two probe ends containing the genomic region of interest. The resulting DNA molecules were circularized by DNA ligase. Unbound linear probes and genomic DNA were removed using exonucleases. The captured regions of interest were bar-coded and amplified in a PCR reaction. Using SPRI bead technology primer dimers were removed. The samples were pooled at a concentration of 2 nM. Sequencing was performed using paired-end sequencing on an Illumina MiSeq platform. Overlapping paired end reads were merged using FLASH2. Merged reads were mapped to the human genome (build hg19; bwa 0.7.5) prior to sorting by amplicon and variant calling per amplicon with GATK HaplotypeCaller (GATK 3.8). The positions in which at least one sample was polymorphic were used to genotype all samples together using GATK GenotypeGVCFs (GATK 3.8). Finally, variants were annotated using ANNOVAR (23-05-2015).

After genotyping, a relationship between polymorphisms and V_T was sought. Therefore, we used the number of copies to create a percentage of variant allele to allow a correlation analysis, using the formula: variant allele (%) = number of copies of variant allele/(number

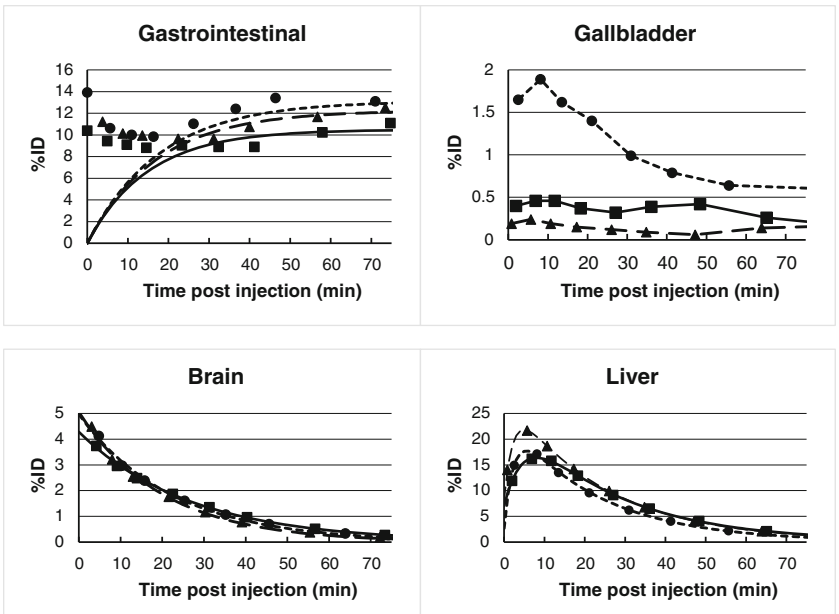

Fig. 2 Mean fractional activities with respect to total body activities in subjects 1, 2 and 3 (Table 1; *circles*, *triangles* and *squares*, respectively) with their respective curve fits (lines) for the brain, gallbladder, intestines and liver

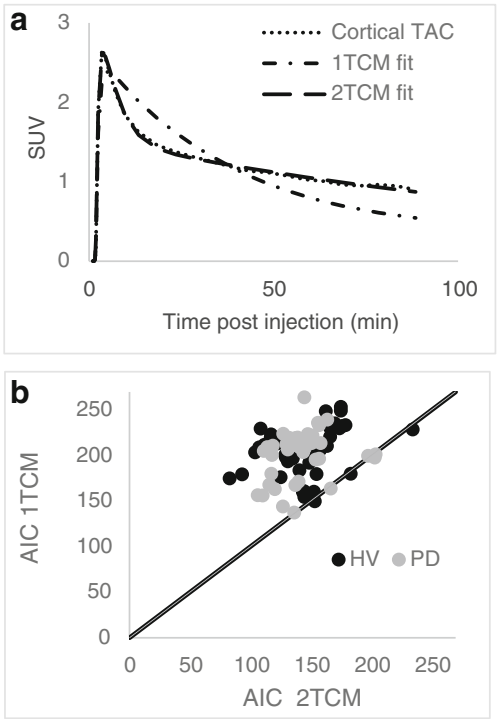

Fig. 3 **a** Representative 1TCM and 2TCM fits for a baseline composite cortical TAC and corresponding arterial blood/plasma input function. **b** 1TCM and 2TCM AIC values for model fitting to the baseline TACs of different brain regions in 10 Parkinson's disease patients (PD) and 11 healthy volunteers (HV)

of copies variant allele + number of copies reference allele). The percentage of variant copies therefore ranged from 0 (homozygote reference) to 1 (homozygote variant). A Spearman's correlation coefficient was calculated using the percentage of variant allele and the composite cortical V_T value – using both individual and average metabolite-corrected input curves. When a retest scan was performed, the average of the test and retest V_T values was used.

General statistics

Conventional statistical analysis was performed with SPSS, version 24.0 (IBM Corp., Armonk, NY, USA) and significance was considered for p values <0.05 after Bonferroni correction for multiple comparisons.

Results

Biodistribution and whole-body dosimetry

Figure 1 shows coronal slices of the WB PET scan biodistribution data over time. The normalized TACs for brain, gallbladder, liver and intestines are shown in Fig. 2. Predominantly hepatobiliary excretion was observed. In Supplementary Table 1, the NCA for all source organs with significant activity uptake are listed with individual organ doses in all subjects with mean values and standard deviations. The organ absorbed doses were the largest for the gallbladder (25 μGy/MBq), liver (22 μGy/MBq) and small intestine (20 μGy/MBq). The average (± standard deviation) ED was 4.47 ± 0.32 μSv/MBq (Supplementary Table 2), which is in the typical range for ^{11}C-radiolabelled ligands (5.7–1.2 μSv/MBq) [22].

Tracer kinetic modelling and test–retest variation

Model selection and assessment of intersubject variation were performed in 10 PD patients and 11 HV (Table 1). Figure 3 shows fitted TACs. Most (> 85%) of the 2TCM AIC values were lower than the 1TCM AIC values (Fig. 3). Therefore, the 2TCM was selected as the optimal model for [^{11}C]JNJ717 and the results reported relate only to the 2TCM V_T values.

Intersubject variation was acceptable with an average V_T of 3.4 ± 0.8 (range 2.0–6.7) in HV (coefficient of variation, CoV,

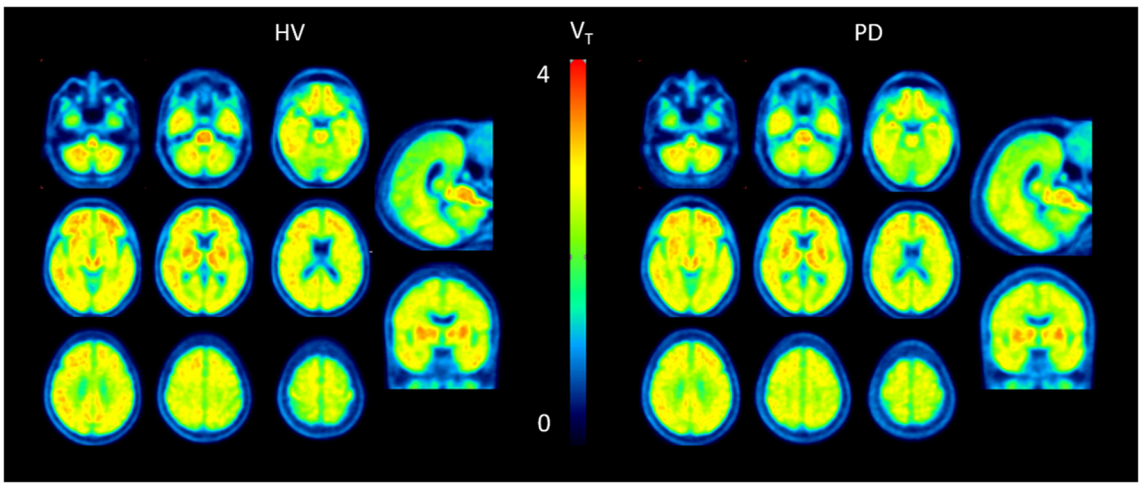

Fig. 4 Average parametric LGA V_T images in healthy volunteers (HV) and Parkinson's disease patients (PD)

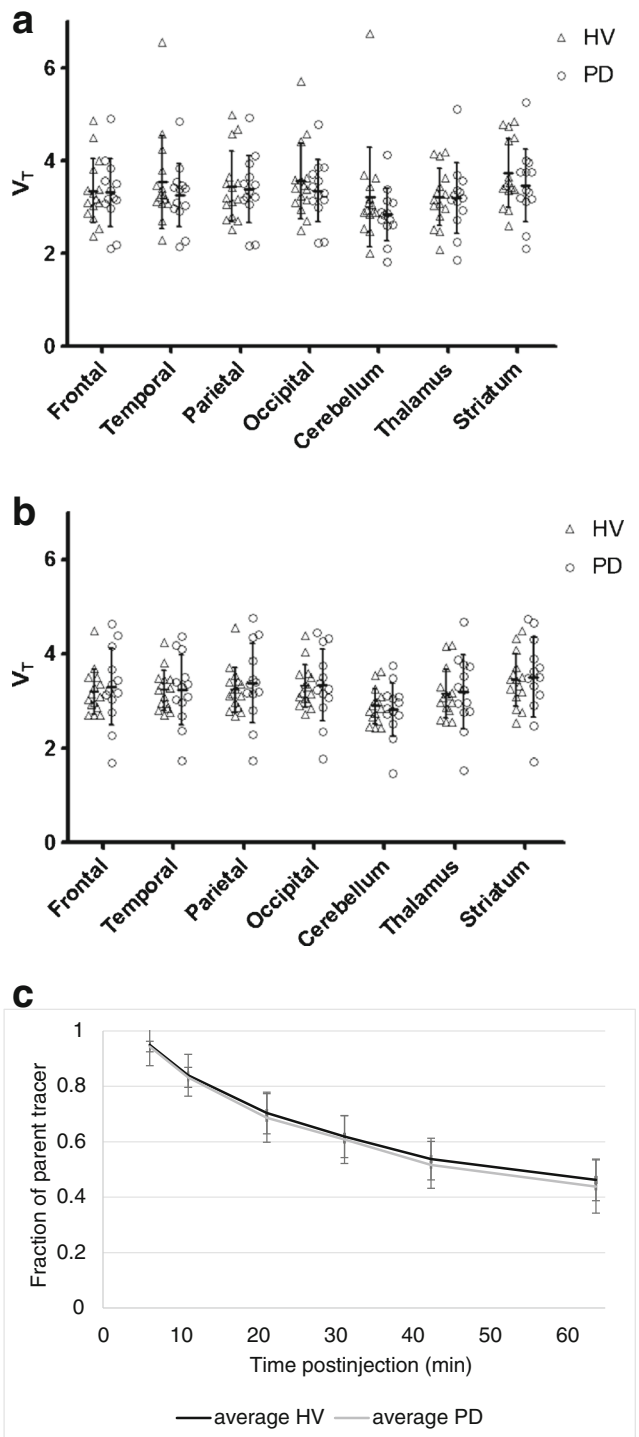

Fig. 5 **a**, **b** V_T values in Parkinson's disease patients (PD) and healthy volunteers (HV) (test and retest combined) using (**a**) individual metabolite curves and (**b**) average metabolite curves. **c** Average metabolite curves with standard deviations in Parkinson's disease patients (PD) and healthy volunteers (HV)

23.8%) and an average V_T of 3.3 ± 0.7 (range 1.8–5.3) in PD patients (CoV 21.7%). Very similar results were obtained using the average metabolite curve: average V_T 3.2 ± 0.5 (range 2.4–4.6) in HV (CoV 15.0%), and 3.2 ± 0.8 (range 1.5–4.7) in PD patients (CoV 23.5%).

V_T showed little variation across most cortical and subcortical brain regions (Figs. 4 and 5), whereas the brainstem and striatum showed slightly higher mean [^{11}C]JNJ717 uptake (about 10%). Regarding the stability of V_T over time, the effects of reducing the acquisition time to 60, 70 and 80 min were calculated in relation to the full 90 min acquisition. The results are shown in Table 2 and Fig. 6. The average biases were acceptable at around 5% for an acquisition time of 70 min: 6.9 ± 8.3% for 2TCM and 4.6 ± 4.1% for LGA for the individual metabolite-corrected input curve, and 3.9 ± 3.7% for 2TCM and 3.7 ± 3.7% for LGA for the average metabolite-corrected input curve. Reducing the acquisition time to 60 min led to individual biases of more than 25% in both cortical and subcortical regions.

TRV was calculated using an acquisition time of 90 min for 2TCM and LGA. The results are shown in Table 3 for various subcortical and cortical brain regions. The average TRV and aTRV values were −4.7% and 12.6% using individual metabolite curves, respectively, and showed no improvement when average metabolite curves were used (−7.7% and 10.2%, respectively). In two subjects, values were higher (30–40%), probably due to the high variation in test–retest metabolite fraction.

[^{11}C]JNJ717 distribution volume in PD patients and healthy volunteers

Neither a VOI-based nor a voxel-based analysis showed significant absolute or relative differences in [^{11}C]JNJ717 distribution volume between PD patients and HV. Whether individual or average metabolite correction input curves were used, did not affect the results.

Genotyping

In total, seven single nucleotide polymorphisms (SNPs) in the 13 exons of the P2X7R were identified, and six were nonsynonymous mutations and one was a synonymous mutation (Table 4). In two PD patients, a lower V_T (around 2 compared to around 3–5) was observed (Fig. 5). One of these patients was homozygous for the variant rs3751143 while the other – although heterozygous – had a much higher number of copies of the variant allele, in contrast to the other heterozygous subjects.

Additionally, Spearman's correlation coefficient between the seven SNPs and the V_T of the composite cortical VOI was calculated. Of these seven, only the reference SNP rs3751143 on exon 13 showed a significant correlation after Bonferroni correction ($\rho_{Spearman}$ = 0–0.60, p = 0.03) using individual metabolite-corrected input curves (Fig. 7a). This correlation remained significant using V_T values calculated with

Table 2 Baseline 2TCM and LGA V_T values with acquisition times of 90, 80, 70 and 60 min using individual metabolite curves and average metabolite curves for different brain regions

Metabolite curves	Brain region	Baseline V_T values							
		2TCM				LGA			
		90 min	80 min	70 min	60 min	90 min	80 min	70 min	60 min
individual	Composite cortical	3.5 ± 0.8 (2.1–5.3)	3.3 ± 0.8 (2.0–4.9)	3.2 ± 0.7 (1.9–4.6)	3.1 ± 0.7 (1.8–4.4)	3.4 ± 0.7 (2.1–4.9)	3.3 ± 0.7 (2.0–4.7)	3.2 ± 0.7 (1.9–4.5)	3.1 ± 0.7 (1.9–4.3)
	Frontal	3.4 ± 0.8 (2.1–5.4)	3.3 ± 0.8 (2.0–5.0)	3.2 ± 0.7 (1.9–4.6)	3.1 ± 0.7 (1.8–4.2)	3.4 ± 0.8 (2.0–4.9)	3.3 ± 0.7 (2.0–4.7)	3.2 ± 0.7 (1.9–4.5)	3.1 ± 0.7 (1.8–4.3)
	Temporal	3.5 ± 0.8 (2.3–5.3)	3.4 ± 0.7 (2.1–4.9)	3.2 ± 0.7 (1.9–4.6)	3.1 ± 0.6 (1.8–4.5)	3.4 ± 0.7 (2.1–4.8)	3.3 ± 0.7 (2.0–4.7)	3.2 ± 0.7 (1.9–4.5)	3.1 ± 0.6 (1.9–4.3)
	Parietal	3.5 ± 0.8 (2.2–5.4)	3.4 ± 0.8 (2.1–5.1)	3.3 ± 0.8 (1.9–4.9)	3.2 ± 0.7 (1.8–4.6)	3.4 ± 0.8 (2.1–4.9)	3.3 ± 0.7 (2.0–4.8)	3.2 ± 0.7 (1.9–4.6)	3.1 ± 0.7 (1.9–4.4)
	Occipital	3.5 ± 0.7 (2.3–5.1)	3.4 ± 0.7 (2.2–4.7)	3.2 ± 0.7 (2.0–4.5)	3.1 ± 0.7 (1.9–4.6)	3.4 ± 0.7 (2.2–4.8)	3.3 ± 0.7 (2.1–4.6)	3.2 ± 0.7 (2.0–4.5)	3.2 ± 0.7 (1.9–4.4)
	Cerebellum	3.1 ± 0.7 (2.0–4.5)	2.9 ± 0.6 (1.8–4.1)	2.8 ± 0.6 (1.7–3.9)	2.7 ± 0.5 (1.6–3.9)	2.9 ± 0.6 (1.8–4.1)	2.9 ± 0.6 (1.7–4.0)	2.8 ± 0.5 (1.6–3.9)	2.7 ± 0.5 (1.6–3.8)
	Striatum	3.9 ± 1.0 (2.2–6.4)	3.7 ± 0.9 (2.0–5.4)	3.5 ± 0.8 (1.9–5.2)	3.4 ± 0.8 (1.9–4.9)	3.5 ± 0.8 (2.1–5.2)	3.5 ± 0.8 (2.0–5.2)	3.4 ± 0.7 (1.9–5.1)	3.3 ± 0.7 (1.9–4.7)
	Corpus callosum	3.6 ± 1.0 (2.1–5.7)	3.4 ± 0.9 (2.0–5.6)	3.4 ± 0.9 (1.8–5.4)	3.3 ± 0.9 (1.8–5.2)	3.3 ± 0.8 (1.9–5.2)	3.2 ± 0.8 (1.9–5.0)	3.1 ± 0.7 (1.7–4.6)	3.0 ± 0.6 (1.7–4.1)
Average	Composite cortical	3.3 ± 0.7 (1.7–4.4)	3.2 ± 0.7 (1.7–4.4)	3.1 ± 0.7 (1.6–4.3)	3.1 ± 0.7 (1.6–4.3)	3.3 ± 0.7 (1.7–4.5)	3.2 ± 0.7 (1.7–4.5)	3.1 ± 0.7 (1.6–4.4)	3.1 ± 0.7 (1.6–4.3)
	Frontal	3.2 ± 0.7 (1.7–4.6)	3.1 ± 0.7 (1.6–4.5)	3.1 ± 0.7 (1.6–4.5)	3.0 ± 0.7 (1.6–4.3)	3.3 ± 0.7 (1.7–4.6)	3.2 ± 0.7 (1.6–4.6)	3.1 ± 0.7 (1.6–4.6)	3.1 ± 0.7 (1.6–4.4)
	Temporal	3.3 ± 0.7 (1.7–4.4)	3.2 ± 0.6 (1.7–4.3)	3.1 ± 0.7 (1.6–4.2)	3.0 ± 0.6 (1.6–4.2)	3.2 ± 0.6 (1.7–4.4)	3.2 ± 0.6 (1.7–4.3)	3.1 ± 0.6 (1.6–4.2)	3.0 ± 0.6 (1.6–4.1)
	Parietal	3.3 ± 0.7 (1.7–4.8)	3.2 ± 0.7 (1.7–4.7)	3.2 ± 0.7 (1.6–4.6)	3.1 ± 0.7 (1.6–4.5)	3.3 ± 0.7 (1.7–4.7)	3.2 ± 0.7 (1.7–4.7)	3.2 ± 0.7 (1.7–4.6)	3.1 ± 0.7 (1.6–4.4)
	Occipital	3.3 ± 0.7 (1.8–4.5)	3.2 ± 0.7 (1.7–4.5)	3.1 ± 0.7 (1.7–4.4)	3.1 ± 0.7 (1.6–4.4)	3.3 ± 0.7 (1.8–4.5)	3.2 ± 0.7 (1.7–4.5)	3.2 ± 0.7 (1.7–4.4)	3.1 ± 0.7 (1.6–4.4)
	Cerebellum	2.8 ± 0.5 (1.5–3.7)	2.8 ± 0.5 (1.4–3.6)	2.7 ± 0.5 (1.4–3.6)	2.8 ± 0.6 (1.4–4.4)	2.8 ± 0.5 (1.5–3.7)	2.8 ± 0.5 (1.4–3.7)	2.7 ± 0.5 (1.4–3.6)	2.7 ± 0.5 (1.4–3.6)
	Striatum	3.6 ± 1.0 (1.7–5.9)	3.5 ± 1.0 (1.7–6.1)	3.4 ± 0.8 (1.6–4.7)	3.3 ± 0.8 (1.6–4.7)	3.4 ± 0.8 (1.7–4.7)	3.4 ± 0.8 (1.7–4.8)	3.3 ± 0.8 (1.6–4.7)	3.3 ± 0.7 (1.6–4.5)
	Corpus callosum	3.4 ± 1.0 (1.6–4.9)	3.4 ± 0.9 (1.6–4.9)	3.3 ± 0.9 (1.5–4.8)	3.3 ± 0.9 (1.5–5.0)	3.1 ± 0.8 (1.6–4.6)	3.0 ± 0.8 (1.5–4.5)	3.0 ± 0.7 (1.5–4.2)	2.9 ± 0.6 (1.4–3.9)

The data presented are mean ± standard deviation (range)

2TCM two-tissue compartment model, *LGA* Logan graphical analysis

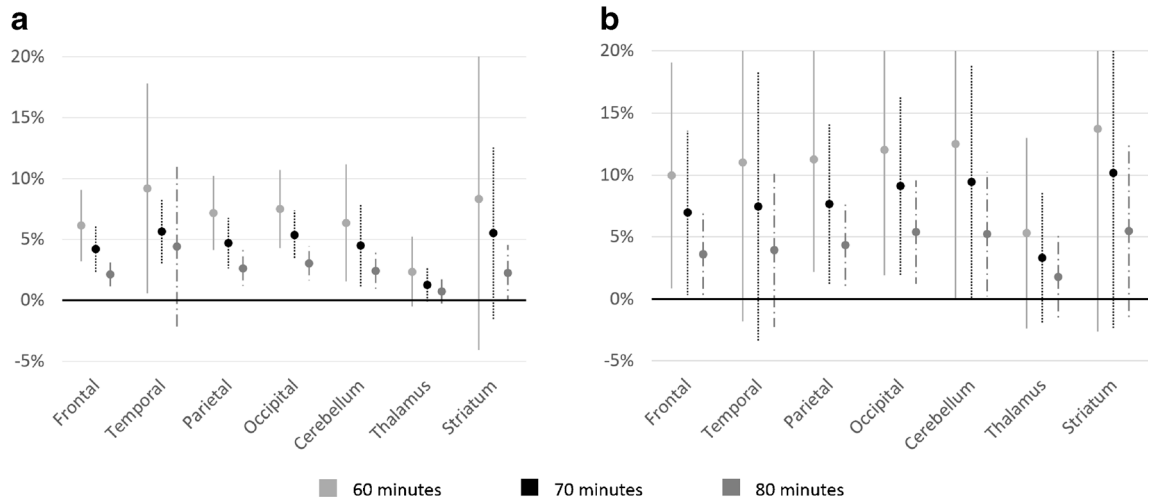

Fig. 6 Percentage differences in V_T values with a reduction in acquisition time to 60 min in relation to the full acquisition time of 90 min in different cortical and subcortical regions (**a** average metabolite curves, **b** individual metabolite curves)

the average metabolite-corrected input curves ($\rho_{Spearman} = -0.70$, $p < 0.01$; Fig. 7b)

Discussion

[^{11}C]JNJ717 is a promising ligand for the study of P2X7R in vivo in the brain using PET imaging. Aside from the shorter half-life of the ^{11}C label that allows multiple single-day scanning, it has characteristics similar to those of its ^{18}F analogue [^{18}F]JNJ64413739 that was recently reported [20, 23]. As well as these two clinically studied radioligands, several others have been developed and studied in preclinical models with variable results [24–32]. [^{11}C]JNJ717 shows moderate uptake in the brain (up to 5% of the injected dose), predominantly hepatobiliary clearance and a typical ^{11}C tracer ED (4.5 μSv/MBq) [22]. As with [^{18}F]JNJ64413739, a reversible 2TCM model fitted the [^{11}C]JNJ717 dynamic PET data reliably, and distribution volume maps could be generated using LGA [20]. Uptake in the grey matter was relatively homogeneous with an acceptable TRV of around 10–15%, again comparable to that of [^{18}F]JNJ64413739 [20]. However, in contrast to [^{18}F]JNJ64413739 [20], the acquisition time could be reduced to 70 min with an acceptable average bias of 5%.

This is the first microglial membrane-bound neuroinflammation marker other than translocator protein receptor (TSPOR) that has been studied using PET in patients with PD. TSPOR and P2X7R are upregulated in activated microglia [33], but P2X7R ligands may allow more specific early detection as P2X7R drives microglial activation [5]. In this study no significant differences in P2X7R expression and distribution between PD patients and HV were observed. A previous study investigating the TSPO ligand [^{11}C]DPA713 showed a significantly higher BP_{nd} (10% to 25% increase) in the occipital, temporal and parietal regions

Table 3 Percentage test–retest variation using individual metabolite curves assessed as $\mathbf{2} \times \left(V_T^{test} - V_T^{retest}\right) / \left(V_T^{test} + V_T^{retest}\right)$ (TRV) and $\mathbf{2} \times \left|V_T^{test} - V_T^{retest}\right| / \left(V_T^{test} + V_T^{retest}\right)$ (aTRV), averaged over the 7 test–retest datasets for different brain regions, together with the between-subject variation of the average test–retest V_T across the seven brain regions

Brain region	V_T (90 min)			
	Individual metabolite curves		Average metabolite curves	
	TRV	aTRV	TRV	aTRV
Cortical	−4.7 (−35.1–32.0)	10.5 (0.0–36.9)	−7.7 (−29.5–9.1)	7.5 (0.3–30.6)
Frontal cortex	−3.9 (−34.4–23.7)	10.8 (0.0–34.4)	−7.0 (−28.1–6.5)	8.9 (2.9–28.1)
Temporal cortex	−4.3 (−35.6–32.1)	13.5 (0.0–35.6)	−8.3 (−28.8–8.5)	10.7 (2.8–28.8)
Parietal cortex	−4.7 (−35.8–26.2)	12.2 (0.0–35.8)	−8.0 (−30.8–7.7)	10.2 (2.8–30.8)
Occipital cortex	−4.0 (−34.3–31.2)	13.3 (0.0–34.3)	−7.7 (−32.1–12.5)	11.3 (2.4–32.1)
Cerebellum	−4.7 (−38.0–26.8)	12.8 (0.0–38.0)	−7.5 (−32.4–7.2)	9.6 (0.2–32.4)
Striatum	−5.9 (−36.9–16.6)	16.9 (0.0–43.8)	−6.8 (−30.6–2.2)	15.3 (10.8–21.7)
Thalamus	−5.5 (−40.6–21.2)	11.7 (0.0–40.6)	−7.7 (−29.5–9.1)	10.3 (2.4–35.2)

The intra-class correlation coefficient is reported as measure for reliability and calculated as (between-subject − within-subject mean sum of squares/(between-subject + within-subject mean sum of squares)

Table 4 Single nucleotide polymorphisms in the 13 exons of the P2X7R

Exon	rs number	Ref	Var	Subject number									
				1	2	3	4	5	6	7	8	9	10
5	rs208294	T	C	Htr (282, 212)	Htr (227, 224)	Htr (231, 262)	Var	Htr (271, 234)	Htr (257, 226)	Ref	Var	Var	Var
8	rs7958311	G	A	Htr (679, 746)	Ref	Htr (718, 787)	Htr (811, 845)	Htr (847, 923)	Htr (571, 661)	Htr (792, 763)	Htr (681, 612)	Htr (748, 888)	Var
8	rs7958316	G	A	Ref	Ref	Ref	Ref	Ref	Ref	Ref	Ref	Ref	Ref
9	G920A	G	A	Ref	Ref	Ref	Ref	Ref	Ref	Ref	Ref	Ref	Htr (169, 221)
11	rs1718119	G	A	Ref	Htr (632, 790)	Htr (768, 852)	Ref	Ref	Ref	Htr (598, 756)	Htr (577,756)	Htr (785, 719)	Ref
13	rs3751143	A	C	Htr (564, 555)	Htr (442, 489)	Ref	Htr (463, 487)	Htr (425, 455)	Htr (371, 436)	Ref	Ref	Ref	Ref
13	Syn, G1746A	G	A	Ref	Htr (319, 221)	Htr (309, 343)	Ref	Ref	Ref	Htr (264, 295)	Htr (345, 329)	Htr (318, 313)	Ref

Exon	Subject number										
	11	12	13	14	15	16	17	18	19	20	21
5	Var	Htr (289, 212)	Htr (283, 217)	Htr (229, 270)	Htr (271, 228)	Htr (82, 82)	Var	Htr (253, 247)	Ref	Var	Ref
8	Ref	Htr (690, 629)	Htr (780, 799)	Ref	Htr (787, 882)	Ref	Var	Ref	Ref	Htr (751, 674)	Var
8	Ref	Ref	Ref	Ref	Ref	Ref	Ref	Ref	Ref	Ref	Htr (211, 206)
9	Ref	Ref	Ref	Ref	Ref	Ref	Ref	Ref	Ref	Ref	Ref
11	Htr (215, 314)	Htr (614, 744)	Ref	Htr (670, 36)	Ref	Ref	Ref	Ref	Htr (495, 762)	Ref	Ref
13	Ref	Ref	Htr (499, 504)	Ref	Htr (535, 523)	Htr (205, 221)	Ref	Var	Htr (286, 447)	Ref	Ref
13	Htr (66, 19)	Htr (251, 335)	Ref	Htr (305,264)	Ref	Ref	Ref	Ref	Htr (130, 207)	Ref	Ref

Values in parentheses are (copies of Ref, copies of Var)

Var homozygous variant, *Ref* homozygous reference, *Htr* heterozygous, *Syn* synonymous single nucleotide variant

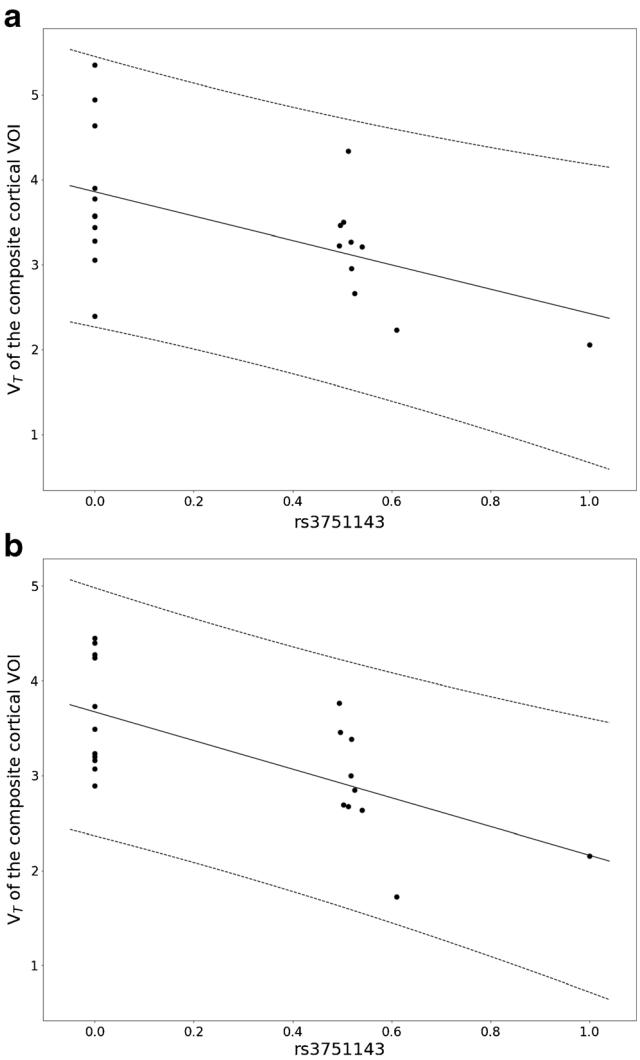

Fig. 7 Correlation between rs3751143 and V_T of the composite cortical VOI with the 95% confidence intervals (*dashed lines*). **a** Using the individual metabolite curves. **b** Using the average metabolite curves

in PD patients than in controls [34]. Similarly, microglial activation has been observed in the pons, basal ganglia and frontal and temporal regions in PD patients using [^{11}C]PK11195 [35, 36]. Furthermore, Ouchi et al. demonstrated parallel changes in midbrain microglial activation with dopaminergic terminal loss in the putamen [37]. Additionally, treatment with AZD3241, a myeloperoxidase inhibitor, has been shown to reduce nigrostriatal [^{11}C]PBR28 binding by about 15% in PD patients [38]. On the other hand, three other previous studies in PD patients using [^{18}F]FEPPA [39, 40] and [^{11}C]PK11195 [41] showed no significant differences. Although results in the latter [^{11}C]PK11195 study were not significant, there was a trend towards increased microglial activation in the putamen and midbrain. Small sample sizes and differences in tracer characteristics may have played a role in the differences in the findings of the various studies ([^{11}C]PK11195 has a low signal-to-noise-ratio) [42, 43].

Preclinical data have shown that pharmacological blockade of P2X7R is advantageous in reversing/diminishing symptomatology in animal models of PD [8, 11]. Moreover, gene expression analysis has shown a small (twofold) increase in the P2X7R gene in RNA extracted from the substantia nigra in PD patients [44]. However, this provides only limited evidence for upregulation of P2X7R in PD [44]. Altered receptor function of P2X7 (e.g. more time in the pore formation stage) without a change in expression levels might also explain the neuroprotective effect of P2X7R antagonism in pharmacological preclinical studies in PD patients. On the other hand, radiotracer affinity compared to the level of P2X7R overexpression may be insufficient to detect subtle group differences, but the expression level of P2X7R under chronic neuroinflammatory conditions in vivo is unknown. Possibly, as P2X7R is believed to orchestrate early microglial activation, P2X7R expression may be higher in patients with prodromal PD. A recent study in a rat model of neuroinflammation using the ^{18}F analogue [^{18}F]JNJ64413739 showed that P2X7R is involved in early microglial activation. The highest signal was observed 2–3 days after lipopolysaccharide injection, after which this effect disappeared. Moreover, increased uptake of [^{18}F]JNJ64413739 was shown to correspond with increased Iba1 staining, a microglial marker, indicating that P2X7R radioligands are probably able to visualize microglial activation [23]. P2X7R function may vary over time, as shown in a mouse model of ALS and a rat model of neuroinflammation, so upregulation may also be transient during the course of neurodegenerative diseases [12, 23]. Therefore, studies in prodromal patients at different disease stages are needed to unravel the distribution of P2X7R during the disease course. Alternatively, as microglial activation in PD may be relatively limited compared to its activation in multiple system atrophy (MSA) [45], future studies in other neurodegenerative diseases such as MSA may provide additional insights. This is supported by the consistent finding of increased microglial activation in atypical parkinsonian syndromes [46–50].

In this study seven SNPs were observed in the subjects. Of these seven, only one (rs3751143) was significantly correlated with composite cortical V_T (Fig. 7). Moreover, the significance remained after accounting for metabolite variation, illustrating the stability of this finding. Genotyping is required for TSPO tracers as the rs6971 polymorphism divides the population into high-, mixed- and low-affinity binders. Our observation could provide preliminary evidence for a similar genotype effect for [^{11}C]JNJ717 binding affinity or may reflect differences in expression level. The rs3751143 polymorphism is known to cause a loss of P2X7R function under normal conditions [51], demonstrating its functional importance. Although homozygous substitution showed a low frequency of 2% and heterozygous substitution a frequency of

20% in that study, this may have been a sample size effect. Therefore, rs3751143 should be investigated in future studies to confirm or reject this genotype effect. Considerable variation in microglial activation among PD patients has been observed in previous studies, and this will be amplified by genotype effects. Therefore, a genotype effect could partly explain the lack of increased P2X7R binding in this group comparison.

This study had some limitations. First, all PD patients were scanned while on medication to facilitate a 90-min scan time because defining the optimal kinetic model was the principal aim of the study. However, no interaction between dopaminomimetics and P2X7R binding is to be expected. Also, in a mouse model of schizophrenia, P2X7R depletion did not change the downregulation of D2 receptors or [^{3}H]dopamine release [52]. Second, because of high observed standard errors for the two last metabolite data points, all analyses were performed using both an individual and an average metabolite fit, but very similar results were obtained, indicating the robustness of the results despite this higher variability in the metabolite correction curve.

Conclusion

[^{11}C]JNJ717 is a promising PET radioligand for quantifying P2X7R expression with sufficient brain uptake and a TRV of 10–15% using a reversible 2TCM. Acquisition time can be reduced to 70 min, facilitating patient comfort. Additionally, a possible genotype effect was identified in rs3751143 (exon 13) which may cause differences in binding affinity or expression level. In a first pilot study in PD patients, [^{11}C]JNJ717 uptake was not different from uptake in HV at the voxel level. However, this radioligand may still be valuable in the evaluation of neurodegenerative and inflammatory diseases to answer important questions about disease pathogenesis, neuroinflammation, microglial activation and prognosis.

Acknowledgments The authors thank Mr. Kwinten Porters and Mr. Jef Van Loock for their contributions to scanning and data handling, the PET radiopharmacy team, the medical physics team of UZ Leuven for their skilled contributions and the Michael J. Fox Foundation for their financial support (PRI-PD project, grant ID 12062).

Disclosures The study was partially sponsored by Michael J. Fox Foundation grant "PRI-PD" (no. 12062), and tracer development was partially sponsored by the EU FP7 project InMind. The precursor for the study was kindly donated by Janssen Pharmaceuticals. K.V.L. and W.V. are Senior Clinical Investigators of the Fund for Scientific Research, Flanders, Belgium (FWO). D.V.W. is a PhD fellow of the FWO.

Compliance with ethical standards

Ethical approval All procedures performed in studies involving human participants were in accordance with the ethical standards of the institutional and/or national research committee and with the principles of the 1964 Declaration of Helsinki and its later amendments or comparable ethical standards.

Informed consent Written informed consent was obtained from all individual participants prior to their inclusion in the study.

Conflicts of interest None.

References

1. Skaper SD, Facci L, Zusso M, Giusti P. An inflammation-centric view of neurological disease: beyond the neuron. Front Cell Neurosci. 2018;12:72.
2. Able SL, Fish RL, Bye H, Booth L, Logan YR, Nathaniel C, et al. Receptor localization, native tissue binding and ex vivo occupancy for centrally penetrant P2X7 antagonists in the rat. Br J Pharmacol. 2011;162(2):405–14.
3. Bhattacharya A, Biber K. The microglial ATP-gated ion channel P2X7 as a CNS drug target. Glia. 2016;64(10):1772–87.
4. Masuch A, Shieh CH, van Rooijen N, van Calker D, Biber K. Mechanism of microglia neuroprotection: involvement of P2X7, TNFalpha, and valproic acid. Glia. 2016;64(1):76–89.
5. Monif M, Burnstock G, Williams DA. Microglia: proliferation and activation driven by the P2X7 receptor. Int J Biochem Cell Biol. 2010;42(11):1753–6.
6. Chen X, Hu J, Jiang L, Xu S, Zheng B, Wang C, et al. Brilliant blue G improves cognition in an animal model of Alzheimer's disease and inhibits amyloid-beta-induced loss of filopodia and dendrite spines in hippocampal neurons. Neuroscience. 2014;279:94–101.
7. Diaz-Hernandez JI, Gomez-Villafuertes R, Leon-Otegui M, Hontecillas-Prieto L, Del Puerto A, Trejo JL, et al. In vivo P2X7 inhibition reduces amyloid plaques in Alzheimer's disease through GSK3beta and secretases. Neurobiol Aging. 2012;33(8):1816–28.
8. Ferrazoli EG, de Souza HD, Nascimento IC, Oliveira-Giacomelli A, Schwindt TT, Britto LR, et al. Brilliant blue G, but not fenofibrate, treatment reverts hemiparkinsonian behavior and restores dopamine levels in an animal model of Parkinson's disease. Cell Transplant. 2017;26(4):669–77.
9. Wang XH, Xie X, Luo XG, Shang H, He ZY. Inhibiting purinergic P2X7 receptors with the antagonist brilliant blue G is neuroprotective in an intranigral lipopolysaccharide animal model of Parkinson's disease. Mol Med Rep. 2017;15(2):768–76.
10. Sluyter R, Bartlett R, Ly D, Yerbury JJ. P2X7 receptor antagonism in amyotrophic lateral sclerosis. Neural Regen Res. 2017;12(5):749–50.
11. Hracsko Z, Baranyi M, Csolle C, Goloncser F, Madarasz E, Kittel A, et al. Lack of neuroprotection in the absence of P2X7 receptors in toxin-induced animal models of Parkinson's disease. Mol Neurodegener. 2011;6:28.
12. Apolloni S, Amadio S, Montilli C, Volonte C, D'Ambrosi N. Ablation of P2X7 receptor exacerbates gliosis and motoneuron death in the SOD1-G93A mouse model of amyotrophic lateral sclerosis. Hum Mol Genet. 2013;22(20):4102–16.
13. Yiangou Y, Facer P, Durrenberger P, Chessell IP, Naylor A, Bountra C, et al. COX-2, CB2 and P2X7-immunoreactivities are increased in activated microglial cells/macrophages of multiple sclerosis and amyotrophic lateral sclerosis spinal cord. BMC Neurol. 2006;6:12.
14. Ory D, Celen S, Gijsbers R, Van Den Haute C, Postnov A, Koole M, et al. Preclinical evaluation of a P2X7 receptor-selective radiotracer: PET studies in a rat model with local overexpression of the

human P2X7 receptor and in nonhuman primates. J Nucl Med. 2016;57(9):1436–41.
15. Fuller SJ, Stokes L, Skarratt KK, Gu BJ, Wiley JS. Genetics of the P2X7 receptor and human disease. Purinergic Signal. 2009;5(2):257–62.
16. Tomlinson CL, Stowe R, Patel S, Rick C, Gray R, Clarke CE. Systematic review of levodopa dose equivalency reporting in Parkinson's disease. Mov Disord. 2010;25(15):2649–53.
17. Stabin MG, Sparks RB, Crowe E. OLINDA/EXM: the second-generation personal computer software for internal dose assessment in nuclear medicine. J Nucl Med. 2005;46(6):1023–7.
18. Johansson L, Mattsson S, Nosslin B, Leide-Svegborn S. Effective dose from radiopharmaceuticals. Eur J Nucl Med. 1992;19(11):933–8.
19. Schramm G, Koole M, Willekens SMA, Rezaei A, Van Weehaeghe D, Delso G, et al. Regional accuracy of ZTE-based attenuation correction in static and dynamic brain PET/MR. Med Phys. 2018. arXiv:1806.03481.
20. Koole M, Schmidt M, Hijzen A, Ravenstijn P, Vandermeulen C, Van Weehaeghe D, et al. (18)F-JNJ-64413739, a novel PET ligand for the P2X7 ion channel: radiation dosimetry, kinetic modeling, test-retest variability and occupancy of the P2X7 antagonist JNJ-54175446. J Nucl Med. 2019;60(5):683–90. https://doi.org/10.2967/jnumed.118.216747.
21. Neveling K, Mensenkamp AR, Derks R, Kwint M, Ouchene H, Steehouwer M, et al. BRCA testing by single-molecule molecular inversion probes. Clin Chem. 2017;63(2):503–12.
22. Zanotti-Fregonara P, Innis RB. Suggested pathway to assess radiation safety of 11C-labeled PET tracers for first-in-human studies. Eur J Nucl Med Mol Imaging. 2012;39(3):544–7.
23. Berdyyeva T, Xia C, Taylor N, He Y, Chen G, Huang C, et al. PET imaging of the P2X7 ion channel with a novel tracer [18F]JNJ-64413739 in a rat model of neuroinflammation. Mol Imaging Biol. 2019. https://doi.org/10.1007/s11307-018-01313-2.
24. Fantoni ER, Dal Ben D, Falzoni S, Di Virgilio F, Lovestone S, Gee A. Design, synthesis and evaluation in an LPS rodent model of neuroinflammation of a novel 18F-labelled PET tracer targeting P2X7. EJNMMI Res. 2017;7(1):31.
25. Gao M, Wang M, Glick-Wilson BE, Meyer JA, Peters JS, Territo PR, et al. Synthesis and initial in vitro characterization of a new P2X7R radioligand [18F]IUR-1602. Appl Radiat Isot. 2018;144:10–8.
26. Han J, Liu H, Liu C, Jin H, Perlmutter JS, Egan TM, et al. Pharmacologic characterizations of a P2X7 receptor-specific radioligand, [11C]GSK1482160 for neuroinflammatory response. Nucl Med Commun. 2017;38(5):372–82.
27. Janssen B, Vugts DJ, Funke U, Spaans A, Schuit RC, Kooijman E, et al. Synthesis and initial preclinical evaluation of the P2X7 receptor antagonist [11C]A-740003 as a novel tracer of neuroinflammation. J Label Compd Radiopharm. 2014;57(8):509–16.
28. Janssen B, Vugts DJ, Wilkinson SM, Ory D, Chalon S, Hoozemans JJM, et al. Identification of the allosteric P2X7 receptor antagonist [11C]SMW139 as a PET tracer of microglial activation. Sci Rep. 2018;8(1):6580.
29. Gao M, Wang M, Glick-Wilson BE, Meyer JA, Peters JS, Territo PR, et al. Synthesis and preliminary biological evaluation of a novel P2X7R radioligand [18F]IUR-1601. Bioorg Med Chem Lett. 2018;28(9):1603–9.
30. Gao M, Wang M, Green MA, Hutchins GD, Zheng QH. Synthesis of [11C]GSK1482160 as a new PET agent for targeting P2X(7) receptor. Bioorg Med Chem Lett. 2015;25(9):1965–70.
31. Jin H, Han J, Resing D, Liu H, Yue X, Miller RL, et al. Synthesis and in vitro characterization of a P2X7 radioligand [123I]TZ6019 and its response to neuroinflammation in a mouse model of Alzheimer disease. Eur J Pharmacol. 2018;820:8–17.
32. Territo PR, Meyer JA, Peters JS, Riley AA, McCarthy BP, Gao M, et al. Characterization of 11C-GSK1482160 for targeting the P2X7 receptor as a biomarker for neuroinflammation. J Nucl Med. 2017;58(3):458–65.
33. Tronel C, Largeau B, Santiago Ribeiro MJ, Guilloteau D, Dupont AC, Arlicot N. Molecular targets for PET imaging of activated microglia: the current situation and future expectations. Int J Mol Sci. 2017;18(4). https://doi.org/10.3390/ijms18040802.
34. Terada T, Yokokura M, Yoshikawa E, Futatsubashi M, Kono S, Konishi T, et al. Extrastriatal spreading of microglial activation in Parkinson's disease: a positron emission tomography study. Ann Nucl Med. 2016;30(8):579–87.
35. Gerhard A, Pavese N, Hotton G, Turkheimer F, Es M, Hammers A, et al. In vivo imaging of microglial activation with [11C](R)-PK11195 PET in idiopathic Parkinson's disease. Neurobiol Dis. 2006;21(2):404–12.
36. Kobylecki C, Counsell SJ, Cabanel N, Wachter T, Turkheimer FE, Eggert K, et al. Diffusion-weighted imaging and its relationship to microglial activation in parkinsonian syndromes. Parkinsonism Relat Disord. 2013;19(5):527–32.
37. Ouchi Y, Yoshikawa E, Sekine Y, Futatsubashi M, Kanno T, Ogusu T, et al. Microglial activation and dopamine terminal loss in early Parkinson's disease. Ann Neurol. 2005;57(2):168–75.
38. Jucaite A, Svenningsson P, Rinne JO, Cselenyi Z, Varnas K, Johnstrom P, et al. Effect of the myeloperoxidase inhibitor AZD3241 on microglia: a PET study in Parkinson's disease. Brain. 2015;138(Pt 9):2687–700.
39. Ghadery C, Koshimori Y, Coakeley S, Harris M, Rusjan P, Kim J, et al. Microglial activation in Parkinson's disease using [18F]-FEPPA. J Neuroinflammation. 2017;14(1):8.
40. Koshimori Y, Ko JH, Mizrahi R, Rusjan P, Mabrouk R, Jacobs MF, et al. Imaging striatal microglial activation in patients with Parkinson's disease. PLoS One. 2015;10(9):e0138721.
41. Bartels AL, Willemsen AT, Doorduin J, de Vries EF, Dierckx RA, Leenders KL. [11C]-PK11195 PET: quantification of neuroinflammation and a monitor of anti-inflammatory treatment in Parkinson's disease? Parkinsonism Relat Disord. 2010;16(1):57–9.
42. Thobois S, Guillouet S, Broussolle E. Contributions of PET and SPECT to the understanding of the pathophysiology of Parkinson's disease. Neurophysiol Clin. 2001;31(5):321–40.
43. Firbank MJ, Yarnall AJ, Lawson RA, Duncan GW, Khoo TK, Petrides GS, et al. Cerebral glucose metabolism and cognition in newly diagnosed Parkinson's disease: ICICLE-PD study. J Neurol Neurosurg Psychiatry. 2017;88(4):310–6.
44. Durrenberger PF, Grunblatt E, Fernando FS, Monoranu CM, Evans J, Riederer P, et al. Inflammatory pathways in Parkinson's disease; a BNE microarray study. Parkinsons Dis. 2012;2012:214714.
45. Lim S, Chun Y, Lee JS, Lee SJ. Neuroinflammation in synucleinopathies. Brain Pathol. 2016;26(3):404–9.
46. Dodel R, Spottke A, Gerhard A, Reuss A, Reinecker S, Schimke N, et al. Minocycline 1-year therapy in multiple-system-atrophy: effect on clinical symptoms and [11C](R)-PK11195 PET (MEMSA-trial). Mov Disord. 2010;25(1):97–107.
47. Gerhard A, Banati RB, Goerres GB, Cagnin A, Myers R, Gunn RN, et al. [11C](R)-PK11195 PET imaging of microglial activation in multiple system atrophy. Neurology. 2003;61(5):686–9.
48. Gerhard A, Trender-Gerhard I, Turkheimer F, Quinn NP, Bhatia KP, Brooks DJ. In vivo imaging of microglial activation with [11C](R)-PK11195 PET in progressive supranuclear palsy. Mov Disord. 2006;21(1):89–93.

49. Gerhard A, Watts J, Trender-Gerhard I, Turkheimer F, Banati RB, Bhatia K, et al. In vivo imaging of microglial activation with [11C](R)-PK11195 PET in corticobasal degeneration. Mov Disord. 2004;19(10):1221–6.
50. Passamonti L, Rodriguez PV, Hong YT, Allinson KSJ, Bevan-Jones WR, Williamson D, et al. [11C]PK11195 binding in Alzheimer disease and progressive supranuclear palsy. Neurology. 2018;90(22):e1989–e96.
51. Gu BJ, Zhang W, Worthington RA, Sluyter R, Dao-Ung P, Petrou S, et al. A Glu-496 to Ala polymorphism leads to loss of function of the human P2X7 receptor. J Biol Chem. 2001;276(14):11135–42.
52. Kovanyi B, Csolle C, Calovi S, Hanuska A, Kato E, Koles L, et al. The role of P2X7 receptors in a rodent PCP-induced schizophrenia model. Sci Rep. 2016;6:36680.